Relativistic approach for the determination of nuclear and neutron star properties in consideration of PREX-II results

Virender Thakur,[1,*] Raj Kumar,[1,†] Pankaj Kumar,[2] Mukul Kumar,[1] C. Mondal,[3] Kaixuan Huang,[4] Jinniu Hu,[4] B. K. Agrawal,[5,‡] and Shashi K. Dhiman[1,6,§]

[1]*Department of Physics, Himachal Pradesh University, Shimla-171005, India*

[2]*Department of Applied Sciences, CGC College of Engineering, Landran, Mohali 140307, India*

[3]*Laboratoire de Physique Corpusculaire, CNRS, ENSICAEN, UMR6534, Université de Caen Normandie, F-14000 Caen Cedex, France*

[4]*School of Physics, Nankai University, Tianjin 300071, China*

[5]*Saha Institute of Nuclear Physics, 1/AF Bidhannagar, Kolkata 700064, India*

[6]*School of Applied Sciences, Himachal Pradesh Technical University, Hamirpur 177001, India*

(Received 15 September 2022; accepted 19 December 2022; published 12 January 2023)

The bulk properties of nuclear matter and neutron stars with the newly generated relativistic interaction Dev Bhoomi Himachal Pradesh (DBHP) are investigated, which provides an opportunity to modify the coupling parameters keeping in view the finite nuclei, nuclear matter, PREX-II data for neutron skin thickness in ^{208}Pb, and astrophysical constraints. The relativistic interaction has been generated by including all possible self and mixed interactions among σ, ω, and ρ mesons up to the quartic order satisfying the naturalness behavior of parameters. A covariance analysis is performed to assess the statistical uncertainties of the model parameters and observables of interest along with correlations amongst them. We obtained a value of neutron skin thickness for the ^{208}Pb nucleus of $\Delta r_{\rm np} = 0.24 \pm 0.02$ fm. The maximum gravitational mass of a neutron star and the radius corresponding to the canonical mass ($R_{1.4}$) come out to be $2.03 \pm 0.04\ M_\odot$ and 13.39 ± 0.41 km, respectively. The dimensionless tidal deformability Λ for a neutron star is also analyzed.

DOI: 10.1103/PhysRevC.107.015803

I. INTRODUCTION

Neutron stars (NSs) are highly dense and asymmetric nuclear systems having a central density about 5-6 times the nuclear saturation density [1]. The studies of the NSs proclaim that their internal structures are quite complex as new degrees of freedom like hyperons and quarks may appear in the core. The NS properties like mass, radius, and tidal deformability can be estimated using equations of state (EOSs) obtained within various theoretical models [2–4]. One of such models is based on the relativistic interaction, which describes the interaction between nucleons through σ, ω, and ρ mesons. There are several models of relativistic mean-field (RMF) effective Lagrangian density consisting of nonlinear σ, ω, and ρ terms and cross terms that have been analyzed for nucleonic and hyperonic matter and confronted with the constraints of nuclear matter properties and astrophysical observations of NS masses [5–9].

The nuclear theory studies [10–12] are mainly focusing on understanding the dense matter in NS. The constraints on EOS at high density are imposed with currently available lower bounds on a neutron star's maximum mass and radius [13–15]. The precise measurement of masses of millisecond pulsars such as PSR J1614-2230 [16] and PSR $J0348 + 0432$ [17] show that the maximum mass of a NS should be around $2\ M_\odot$. The recent observations with LIGO and Virgo of GW170817 event [18,19] of Binary Neutron Stars merger and the discovery of NS with masses around $2\ M_\odot$ [16,17,20–23] have intensified the interest in these intriguing objects. The analysis of GW170817 has demonstrated the potential of gravitational wave (GW) observations to yield new information relating to the limits on NS tidal deformability. The Lead Radius Experiment (PREX-II) has recently provided a model-independent extraction of neutron skin thickness of ^{208}Pb as $\Delta r_{\rm np} = 0.283 \pm 0.071$ fm [24]. The $\Delta r_{\rm np}$ has been identified as an ideal probe for the density dependence of symmetry energy—a key but poorly known quantity that describes the isospin dependence of the EOS of asymmetric nuclear matter and plays a critical role in various issues in nuclear physics and astrophysics. The neutron skin thickness of the lead nucleus exhibits a strong positive linear correlation with the slope of the symmetry energy parameter (L) at saturation density. The parameter L that determines the density dependence of the symmetry energy strongly affects the mass-radius relation and tidal deformability (Λ) of a neutron star and provides a unique bridge between atomic nuclei and neutron stars [25]. The large value of $\Delta r_{\rm np} = 0.283 \pm 0.071$ fm suggests a large value of L, which yields a very stiff EOS. This generally gives rise to a large value of neutron star radius and the tidal deformability [3]. The upper limit on $\Lambda_{1.4} \leqslant 580$

*virenthakur2154@gmail.com
†raj.phy@gmail.com
‡sinp.bijay@gmail.com
§shashi.dhiman@gmail.com

for GW170817 requires softer EOSs and hence softer symmetry energy coefficients [18]. The heaviest observed neutron star $M_{\rm max} = 2.35 \pm 0.17\ M_\odot$ for the black-widow pulsar PSR J0952-0607 [26] may place stringent constraints on the symmetry energy at high densities, since the EOS of symmetric nuclear matter from heavy-ion collision flow data [27] that is relatively soft and limits the NS maximum mass.

The motivation of the present work is to generate a new parametrization of the RMF model that can accommodate the properties of NSs within the astrophysical observations without compromising the finite nuclei properties. The RMF model used in the present work includes all possible self and mixed-coupling terms for the σ, ω, and ρ mesons up to the quartic order so that the parameters should obey the naturalness behavior as imposed by the effective field theory [28]. In this work, the new parameter set is searched in view of PREX-II data and the model EOS satisfies the observed astrophysical constraints imposed by NSs.

The paper is organized as follows, in Sec. II, the theoretical framework that is used to construct the EOS for neutron stars has been discussed. In Sec. III, the procedure for optimization and covariance analysis of the parameters is discussed. In Sec. IV, we present our results. Finally, we summarize the results of the present work in Sec. V.

II. THEORETICAL MODEL

The effective Lagrangian density for the RMF model generally describes the interaction of the baryons via the exchange of σ, ω, and ρ mesons up to the quartic order. The Lagrangian density [5,7,29] is given by

$$\begin{aligned}\mathcal{L} = &\sum_B \overline{\Psi}_B[i\gamma^\mu\partial_\mu - (M_B - g_{\sigma B}\sigma) - (g_{\omega B}\gamma^\mu\omega_\mu \\ &+ \frac{1}{2}g_{\rho B}\gamma^\mu\tau_B.\rho_\mu)]\Psi_B + \frac{1}{2}(\partial_\mu\sigma\partial^\mu\sigma - m_\sigma^2\sigma^2) \\ &- \frac{\overline{\kappa}}{3!}g_{\sigma N}^3\sigma^3 - \frac{\overline{\lambda}}{4!}g_{\sigma N}^4\sigma^4 - \frac{1}{4}\omega_{\mu\nu}\omega^{\mu\nu} + \frac{1}{2}m_\omega^2\omega_\mu\omega^\mu \\ &+ \frac{1}{4!}\zeta g_{\omega N}^4(\omega_\mu\omega^\mu)^2 - \frac{1}{4}\rho_{\mu\nu}\rho^{\mu\nu} + \frac{1}{2}m_\rho^2\rho_\mu\rho^\mu \\ &+ \frac{1}{4!}\xi g_{\rho N}^4(\rho_\mu\rho^\mu)^2 \\ &+ g_{\sigma N}g_{\omega N}^2\sigma\omega_\mu\omega^\mu\left(a_1 + \frac{1}{2}a_2 g_{\sigma N}\sigma\right) \\ &+ g_{\sigma N}g_{\rho N}^2\sigma\rho_\mu\rho^\mu\left(b_1 + \frac{1}{2}b_2 g_{\sigma N}\sigma\right) \\ &+ \frac{1}{2}c_1 g_{\omega N}^2 g_{\rho N}^2\omega_\mu\omega^\mu\rho_\mu\rho^\mu. \end{aligned} \tag{1}$$

The equations of motion for baryons, mesons, and photons can be derived from the Lagrangian density defined in Eq. (1). The equation of motion for baryons can be given as

$$\left[\gamma^\mu\left(i\partial_\mu - g_{\omega B}\omega_\mu - \frac{1}{2}g_{\rho B}\tau_B.\rho_\mu - e\frac{1+\tau_{3B}}{2}A_\mu\right) - (M_B + g_{\sigma B}\sigma)\right]\Psi_B = \epsilon_B\Psi_B. \tag{2}$$

The Euler-Lagrange equations for the ground-state expectation values of the meson fields are

$$\begin{aligned}(-\Delta + m_\sigma^2)\sigma = &\sum_B g_{\sigma B}\rho_{sB} - \frac{\overline{\kappa}}{2}g_{\sigma N}^3\sigma^2 - \frac{\overline{\lambda}}{6}g_{\sigma N}^4\sigma^3 \\ &+ a_1 g_{\sigma N}g_{\omega N}^2\omega^2 + a_2 g_{\sigma N}^2 g_{\omega N}^2\sigma\omega^2 \\ &+ b_1 g_{\sigma N}g_{\rho B}^2\rho^2 + b_2 g_{\sigma N}^2 g_{\rho N}^2\sigma\rho^2, \end{aligned} \tag{3}$$

$$\begin{aligned}(-\Delta + m_\omega^2)\omega = &\sum_B g_{\omega B}\rho_B - \frac{\zeta}{6}g_{\omega N}^4\omega^3 \\ &- 2a_1 g_{\sigma N}g_{\omega N}^2\sigma\omega - a_2 g_{\sigma N}^2 g_{\omega N}^2\sigma^2\omega \\ &- c_1 g_{\omega N}^2 g_{\rho N}^2\omega\rho^2, \end{aligned} \tag{4}$$

$$\begin{aligned}(-\Delta + m_\rho^2)\rho = &\sum_B g_{\rho B}\tau_{3B}\rho_B - \frac{\xi}{6}g_{\rho N}^4\rho^3 \\ &- 2b_1 g_{\sigma N}g_{\rho N}^2\sigma\rho - b_2 g_{\sigma N}^2 g_{\rho N}^2\sigma^2\rho \\ &- c_1 g_{\omega N}^2 g_{\rho N}^2\omega^2\rho, \end{aligned} \tag{5}$$

$$-\Delta A_0 = e\rho_p, \tag{6}$$

where the baryon vector density ρ_B, scalar density ρ_{sB}, and charge density ρ_p are, respectively,

$$\rho_B = \langle\overline{\Psi}_B\gamma^0\Psi_B\rangle = \frac{\gamma k_B^3}{6\pi^2}, \tag{7}$$

$$\rho_{sB} = \langle\overline{\Psi}_B\Psi_B\rangle = \frac{\gamma}{(2\pi)^3}\int_0^{k_B} d^3k\frac{M_B^*}{\sqrt{k^2 + M_B^{*2}}}, \tag{8}$$

$$\rho_p = \left\langle\overline{\Psi}_B\gamma^0\frac{1+\tau_{3B}}{2}\Psi_B\right\rangle, \tag{9}$$

with γ being the spin-isospin degeneracy. Here $M_B^* = M_B - g_{\sigma B}\sigma$ is the effective mass of the baryon species B, k_B is its Fermi momentum, and τ_{3B} denotes the isospin projections of baryon B. The energy density of the uniform matter within the framework of the RMF model is given by

$$\begin{aligned}\mathcal{E} = &\sum_{j=B,\ell}\frac{1}{\pi^2}\int_0^{k_j} k^2\sqrt{k^2 + M_j^{*2}}dk \\ &+ \sum_B g_{\omega B}\omega\rho_B + \sum_B g_{\rho B}\tau_{3B}\rho_B\rho + \frac{1}{2}m_\sigma^2\sigma^2 \\ &+ \frac{\overline{\kappa}}{6}g_{\sigma N}^3\sigma^3 + \frac{\overline{\lambda}}{24}g_{\sigma N}^4\sigma^4 - \frac{\zeta}{24}g_{\omega N}^4\omega^4 \\ &- \frac{\xi}{24}g_{\rho N}^4\rho^4 - \frac{1}{2}m_\omega^2\omega^2 - \frac{1}{2}m_\rho^2\rho^2 \\ &- a_1 g_{\sigma N}g_{\omega N}^2\sigma\omega^2 - \frac{1}{2}a_2 g_{\sigma N}^2 g_{\omega N}^2\sigma^2\omega^2 \\ &- b_1 g_{\sigma N}g_{\rho N}^2\sigma\rho^2 - \frac{1}{2}b_2 g_{\sigma N}^2 g_{\rho N}^2\sigma^2\rho^2 \\ &- \frac{1}{2}c_1 g_{\omega N}^2 g_{\rho N}^2\omega^2\rho^2. \end{aligned} \tag{10}$$

The pressure of the uniform matter is given by

$$
\begin{aligned}
P = & \sum_{j=B,\ell} \frac{1}{3\pi^2} \int_0^{k_j} \frac{k^4 dk}{\sqrt{k^2 + M_j^{*2}}} - \frac{1}{2} m_\sigma^2 \sigma^2 \\
& - \frac{\overline{\kappa}}{6} g_{\sigma N}^3 \sigma^3 - \frac{\overline{\lambda}}{24} g_{\sigma N}^4 \sigma^4 + \frac{\zeta}{24} g_{\omega N}^4 \omega^4 \\
& + \frac{\xi}{24} g_{\rho N}^4 \rho^4 + \frac{1}{2} m_\omega^2 \omega^2 + \frac{1}{2} m_\rho^2 \rho^2 \\
& + a_1 g_{\sigma N} g_{\omega N}^2 \sigma \omega^2 + \frac{1}{2} a_2 g_{\sigma N}^2 g_{\omega N}^2 \sigma^2 \omega^2 \\
& + b_1 g_{\sigma N} g_{\rho N}^2 \sigma \rho^2 + \frac{1}{2} b_2 g_{\sigma N}^2 g_{\rho N}^2 \sigma^2 \rho^2 \\
& + \frac{1}{2} c_1 g_{\omega N}^2 g_{\rho N}^2 \omega^2 \rho^2 . \qquad (11)
\end{aligned}
$$

Here, the sum is taken over nucleons and leptons.

III. OPTIMIZATION AND COVARIANCE ANALYSIS

The optimization of the parameters (**p**) appearing in the Lagrangian [Eq. (1)] has been performed by using the simulated annealing method [30,31] by following the χ^2 minimization procedure, which is given as

$$
\chi^2(\mathbf{p}) = \frac{1}{N_d - N_p} \sum_{i=1}^{N_d} \left(\frac{M_i^{\rm exp} - M_i^{\rm th}}{\sigma_i} \right)^2 , \qquad (12)
$$

where N_d is the number of experimental data points and N_p is the number of fitted parameters. The σ_i denotes adopted errors [32] and $M_i^{\rm exp}$ and $M_i^{\rm th}$ are the experimental and the corresponding theoretical values, respectively, for a given observable. The minimum value of χ_0^2 corresponds to the optimal values $\mathbf{p}_0$ of the parameters. Following the optimization of the energy density functional, it is important to explore the richness of the covariance analysis. It enables one to calculate the statistical uncertainties on model parameters or any calculated physical observables. The covariance analysis also provides additional information about the sensitivity of the parameters to the physical observables and about interdependence among the parameters [32–35]. Having obtained the parameter set, the correlation coefficient between the two quantities Y and Z can be calculated by covariance analysis [32,34–37] as

$$
c_{YZ} = \frac{\overline{\Delta Y \Delta Z}}{\sqrt{\overline{\Delta Y^2}\ \overline{\Delta Z^2}}}, \qquad (13)
$$

where the covariance between Y and Z is expressed as

$$
\overline{\Delta Y \Delta Z} = \sum_{\alpha\beta} \left(\frac{\partial Y}{\partial p_\alpha} \right)_{\mathbf{p}_0} C_{\alpha\beta}^{-1} \left(\frac{\partial Z}{\partial p_\beta} \right)_{\mathbf{p}_0} . \qquad (14)
$$

Here, $C_{\alpha\beta}^{-1}$ is an element of the inverted curvature matrix given by

$$
C_{\alpha\beta} = \frac{1}{2} \left(\frac{\partial^2 \chi^2(\mathbf{p})}{\partial p_\alpha \partial p_\beta} \right)_{\mathbf{p}_0} . \qquad (15)
$$

The standard deviation, $\overline{\Delta Y^2}$, in Y can be computed using Eq. (14) by substituting $Z = Y$. The prediction of the maximum mass around 2 $M_\odot$ for the nonrotating neutron star and the constraints on EOSs of symmetric nuclear matter (SNM) and pure neutron matter (PNM) as extracted from the analysis of particle flow in heavy-ion collisions [27] require relatively softer EOSs as demanded by the GW170817 event.

IV. RESULTS AND DISCUSSION

The parameters of the model are searched by fit to the available experimental data of total binding energies and charge rms radii [38–40] for some closed/open shell nuclei ^{16,24}O, ^{40,48,54}Ca, ^{56,68,78}Ni, ^{88}Sr, ^{90}Zr, ^{100,116,132,138}Sn, ^{144}Sm, and ^{208}Pb. We have also included the maximum mass of the neutron star [41] in our fit data. Recently, the parity-violating electron scattering experiment (PREX-II) put a limit on the neutron skin thickness of ^{208}Pb of $\Delta r_{\rm np} = 0.283 \pm 0.071$ fm [24]. We included the recently measured $\Delta r_{\rm np}$ in our fit data to constrain the linear density dependence of the symmetry energy coefficient. For the open shell nuclei, the pairing has been included by using BCS formalism with constant pairing gaps that have been taken from the particle separation energies of neighboring nuclei [42–44]. In Table I, we display the values of relativistic parametrization DBHP generated for the Lagrangian given by Eq. (1) along with theoretical uncertainties. The values of parameter sets for NL3 [45], FSUGarnet [33], IOPB-1 [46], and Big Apple [35] are also shown.

The effective field theory imposes the condition of naturalness [28] on the parameters or expansion coefficients appearing in the effective Lagrangian density equation (1). According to naturalness, the coefficients of various terms in the Lagrangian density functional should be of the same size when expressed in an appropriate dimensionless ratio. The dimensionless ratios are obtained by dividing Eq. (1) by M^4 and expressing each term in powers of $\frac{g_\sigma \sigma}{M}$, $\frac{g_\omega \omega}{M}$, and $2\frac{g_\rho \rho}{M}$. This means that the dimensionless ratios $\frac{1}{2C_\sigma^2 M^2}$, $\frac{1}{2C_\omega^2 M^2}$, $\frac{1}{8C_\rho^2 M^2}$, $\frac{\overline{\kappa}}{6M}$, $\frac{\overline{\lambda}}{24}$, $\frac{\zeta}{24}$, $\frac{a_1}{M}$, $\frac{a_2}{2}$, $\frac{b_1}{4M}$, $\frac{b_2}{8}$, and $\frac{c_1}{8}$ should be roughly of the same size, where ${c_i}^2 = \frac{{g_i}^2}{{M_i}^2}$, i denotes σ, ω, and ρ mesons. In Table II, we present the overall naturalness behavior of DBHP parametrization, i.e., the value of these parameters when expressed in dimensionless ratios as shown just above. We also display the corresponding values for NL3, FSUGarnet, IOPB-1, and Big Apple parameter sets. It is obvious from the table that DBHP parametrization closely favors the naturalness behavior. This may be attributed to the fact that this parametrization includes all possible self and crossed interaction terms of σ, ω, and ρ mesons up to the quartic order.

The small value of parameter c_1 for the DBHP model that gives rise to better naturalness behavior of the parameters might be attributed to the fact that the coupling parameter c_1 has strong correlation with b_1 and also has good correlation with a_2 and b_2 (see Fig. 1). It is evident from Table I that the value of the coupling parameter c_1 (crossed interaction term of ω^2 and ρ^2) appearing in Eq. (1) is large for IOPB-I,

TABLE I. New parameter set for the DBHP model of the RMF Lagrangian given in Eq. (1) along with theoretical uncertainties. The parameters $\overline{\kappa}$, a_1, and b_1 are in fm^{-1}. The masses m_σ, m_ω, and m_ρ are in MeV. The mass for the nucleon is taken as $M_N = 939$ MeV. The values of $\overline{\kappa}$, $\overline{\lambda}$, a_1, a_2, b_1, b_2, and c_1 are multiplied by 10^2. Parameters for NL3, FSUGarnet, IOPB-1, and Big Apple are also shown for comparison.

Parameters	DBHP	NL3	FSUGarnet	IOPB-1	Big Apple
$\mathbf{g}_\sigma$	10.34155 ± 0.06660	10.21743	10.50315	10.41851	9.67810
$\mathbf{g}_\omega$	13.30826 ± 0.10044	12.86762	13.69695	13.38412	12.33541
$\mathbf{g}_\rho$	11.25845 ± 1.31969	8.94800	13.87880	11.11560	14.14256
$\overline{\kappa}$	1.82166 ± 0.05101	1.95734	1.65229	1.85581	2.61776
$\overline{\lambda}$	0.24446 ± 0.17154	−1.59137	−0.03533	−0.07552	−2.16586
ζ	0.02156 ± 0.00401	0.00000	0.23486	0.01744	0.00070
$\mathbf{a_1}$	0.01172 ± 0.00383	0.00000	0.00000	0.00000	0.00000
$\mathbf{a_2}$	0.05281 ± 0.03677	0.00000	0.00000	0.00000	0.00000
$\mathbf{b_1}$	0.39811 ± 0.40926	0.00000	0.00000	0.00000	0.00000
$\mathbf{b_2}$	0.09412 ± 1.85465	0.00000	0.00000	0.00000	0.00000
$\mathbf{c_1}$	0.79914 ± 3.15145	0.00000	8.60000	4.80000	9.40000
$\mathbf{m}_\sigma$	501.04834 ± 1.34831	508.19400	496.73100	500.48700	492.97500
$\mathbf{m}_\omega$	782.50000	782.50100	782.18700	782.18700	782.18700
$\mathbf{m}_\rho$	770.00000	763.00000	762.46800	762.46800	762.46800

FSU-Garnet, and Big Apple, which shows deviation from the naturalness behavior in the absence of all other possible mixed interaction terms of σ, ω, and ρ mesons. Keeping in view the naturalness behavior of the parameters as imposed by the effective field theory [28] and as observed in the case of the DBHP model, it is important to incorporate the contributions of the higher-order mixed interactions of mesons in the Lagrangian. The naturalness behavior of parameters can be further improved by considering the next higher-order terms containing the gradient of fields [28]. As far as NL3 parametrization is concerned, the naturalness behavior is favored very well but it does not include any cross interaction terms of σ, ω, and ρ mesons, which are very important for constraining the symmetry energy and its density dependence.

In Fig. 1, the correlation coefficients between the DBHP model parameter appearing in the Lagrangian [Eq. (1)] are shown in graphical form. A strong correlation is found between the pairs of model parameters g_σ and g_ω (0.95), c_1 and b_1 (0.80), and a_2 and $\overline{\kappa}$ (0.72). The strong correlation is also found for g_ρ with b_1 and b_2. Mild correlations exist between the pairs of model parameters g_σ and $\overline{\kappa}$, g_σ and a_1, and g_σ and a_2. A strong correlation between the model parameters implies a strong interdependence; i.e., if one parameter is fixed at a certain value then the other must attain the precise value as suggested by their correlation.

A. Properties of finite nuclei and nuclear matter

The newly generated DBHP parametrization gives a good fit to the properties of finite nuclei. In Fig. 2, we display the value of the relative error in the total binding energies $\delta E = \frac{B^{\rm exp} - B^{\rm th}}{B^{\rm exp}}$ calculated for DBHP parametrization. We also display similar results for other parameter sets considered. It is evident that binding energies obtained using DBHP parametrization are in good agreement with the available experimental data [38]. The rms error in total binding energy for all the nuclei

TABLE II. The values of parameters are expressed as dimensionless ratios corresponding to naturalness behavior. All values have been multiplied by 10^3.

Parameters	DBHP	NL3	FSUGarnet	IOPB-1	Big Apple
$\frac{1}{2C_\sigma^2 M^2}$	1.3311	1.4028	1.2690	1.3086	1.4698
$\frac{1}{2C_\omega^2 M^2}$	1.9604	2.0970	1.8508	1.9383	2.2819
$\frac{1}{8C_\rho^2 M^2}$	0.6631	1.0306	0.4278	0.6670	0.4121
$\frac{\overline{\kappa}}{6M}$	0.6380	0.6855	0.5787	0.6499	0.9168
$\frac{\overline{\lambda}}{24}$	0.1018	−0.6630	−0.1472	−0.3146	−0.9024
$\frac{\zeta}{24}$	0.8982	–	0.9785	0.7267	0.0291
$\frac{a_1}{M}$	0.1172	–	–	–	–
$\frac{a_2}{2}$	0.2641	–	–	–	–
$\frac{b_1}{4M}$	0.9953	–	–	–	–
$\frac{b_2}{8}$	0.1177	–	–	–	–
$\frac{c_1}{8}$	0.9989	–	10.7500	6.0000	11.7500

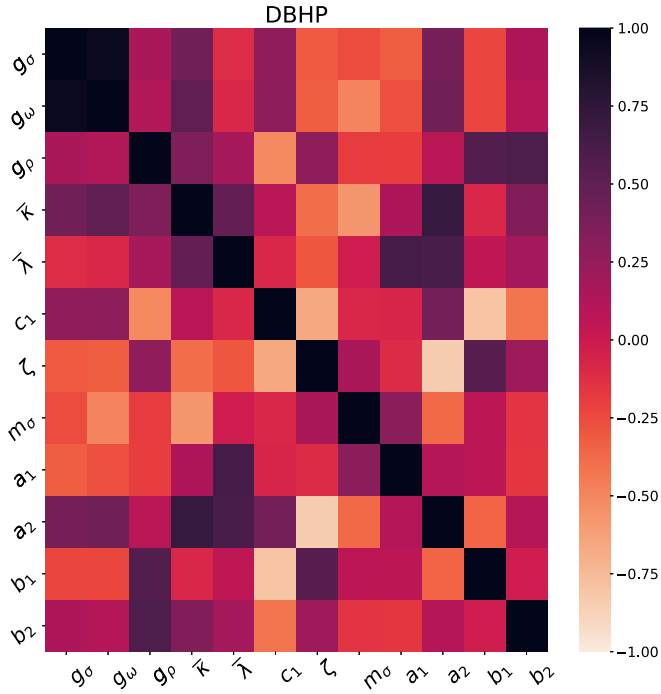

FIG. 1. Correlation coefficients among the model parameters for DBHP parametrization of the Lagrangian given by Eq. (1).

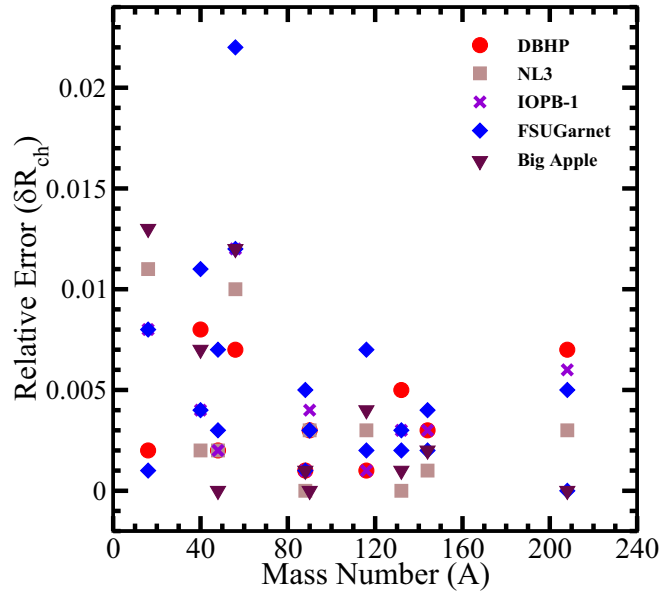

FIG. 3. Relative error in the charge root mean square ($\delta R_{\rm ch}$) plotted against the mass number (A) for the newly generated parameter set DBHP For comparison, the values obtained with parameters NL3, IOPB-1, FSUGarnet, and Big Apple are also displayed.

considered in our fit data is found to be 2.1 MeV. In Fig. 3, we present our results for the relative error $\delta R_{\rm ch}$ for charge rms radii and also compare them with other parameter sets. The rms error in charge radii for all nuclei taken in our fit is 0.02 fm. The neutron skin thickness of ^{208}Pb for the DBHP model comes out to be 0.24 ± 0.02 fm. In Table III, we present

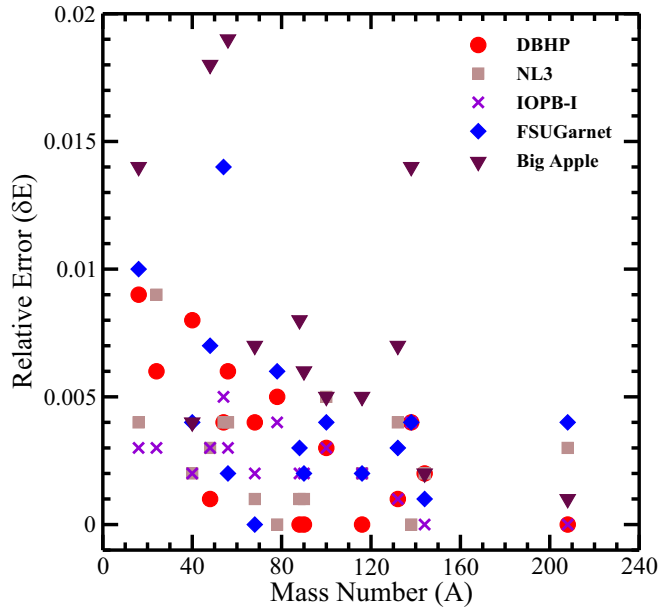

FIG. 2. Relative error in the total binding energy (δE) plotted against the mass number (A) for the newly generated parameter set DBHP. For comparison, the values of δE obtained with parameters NL3, IOPB-1, FSUGarnet, and Big Apple are also displayed.

the results for the SNM properties such as the binding energy per nucleon (E/A), the incompressibility (K), the effective nucleon mass (M^*) at the saturation density (ρ_0), the symmetry energy coefficient (J), the slope of the symmetry energy (L), and the curvature parameter $K_{\rm sym}$ along with the theoretical uncertainties. It is observed that the isoscalar properties (E/A, K, M^*, ρ_0) are well constrained for DBHP parametrization (at the $\leqslant$3.3% level). However, in the isovector sector, the error on the density dependence of the symmetry energy is relatively larger for L ($\approx$23%). The value of $K_{\rm sym}$ is determined only poorly [47–49]. The experimental data on finite nuclei are not enough to constrain $K_{\rm sym}$. Only the accurate knowledge of the symmetry energy at higher densities ($\rho > 2\rho_0$) may constrain the $K_{\rm sym}$ in tighter bounds. This may be attributed to the large experimental error on the neutron skin thickness for ^{208}Pb (0.283 ± 0.071 fm), which leads us to choose the large adopted error during the optimization procedure. The values of neutron skin thickness ($\Delta r_{\rm np}$) for ^{208}Pb and ^{48}Ca nuclei are also presented. The DBHP parameter significantly overestimates the value of neutron skin thickness for ^{48}Ca in comparison to that of $\Delta r_{\rm np}(^{48}{\rm Ca}) = 0.121 \pm 0.026$ fm as reported recently by CREX [50]. Other parametrizations considered in Table III also do not satisfy simultaneously the experimental data for the neutron skin for the ^{208}Pb and ^{48}Ca nuclei. Similar trends have been observed in recent investigations based on the relativistic and nonrelativistic mean-field models, which call for further experimental studies [51–53].

The results are also compared with the NL3 [45], FSUGarnet [33], IOPB-1 [46], and Big Apple [35] parameter sets. These SNM properties are very important for constructing the EOS for nuclear matter. E/A is -16.1 MeV for the DBHP parametrization. The values of J and L obtained by DBHP parametrization are consistent with the values

TABLE III. The bulk nuclear matter properties (NMPs) at saturation density along with calculated theoretical errors for DBHP parametrization compared with that of other parameter sets. ρ_0, E/A, K, M^*/M, J, L, and $K_{\rm sym}$ denote the saturation density, the binding energy per nucleon, the nuclear matter incompressibility coefficient, the ratio of the effective nucleon mass to the nucleon mass, the symmetry energy, the slope of the symmetry energy, and the curvature of the symmetry energy, respectively. The value of ρ_0 is in fm^{-3} and the rest of the quantities are in MeV. The values of the neutron skin thickness $\Delta r_{\rm np}$ for ^{208}Pb and ^{48}Ca nuclei in units of fm are also listed.

NMPs	DBHP	NL3	FSUGarnet	IOPB-1	Big Apple
ρ_0	0.148 ± 0.003	0.148	0.153	0.149	0.155
E/A	-16.11 ± 0.05	-16.25	-16.23	-16.09	-16.34
K	229.5 ± 5.6	271.6	229.6	222.6	227.1
M^*/M	0.615 ± 0.007	0.595	0.578	0.595	0.608
J	34.7 ± 1.5	37.4	30.9	33.3	31.4
L	83.9 ± 19.2	118.6	50.9	63.8	40.3
$K_{\rm sym}$	-33.2 ± 64.1	100.7	57.9	-38.4	88.8
$\Delta r_{\rm np}$ (^{208}Pb)	0.24 ± 0.02	0.28	0.16	0.22	0.15
$\Delta r_{\rm np}$ (^{48}Ca)	0.21 ± 0.02	0.23	0.17	0.17	0.17

$J = 38.1 \pm 4.7$ MeV and $L = 106 \pm 37$ MeV as inferred by Reed *et al.* [3]. The value of K is 225 MeV, which is in agreement with the value of $K = 240 \pm 20$ MeV determined from isoscalar giant monopole resonance for ^{90}Zr and ^{208}Pb nuclei [54,55].

In Fig. 4, we plot the EOS, i.e., pressure as a function of the baryon density for SNM (upper panel) and PNM (lower panel) using the DBHP parametrization that agrees reasonably well and lies in the allowed region with the EOSs extracted from the analysis of the particle flow in heavy-ion collision [27]. It is evident from Fig. 4 that the EOSs for SNM and PNM calculated with the NL3 parametrization are very stiff and ruled out by the heavy-ion collision data. The EOS calculated by using the DBHP parametrization is relatively softer, which is a requirement to constrain the recent astrophysical observations [41,56–58]. In Fig. 5, we plot the symmetry energy as a function of baryon density for the DBHP model. The results for other parametrizations are also shown for comparison. It can be observed that the symmetry energy increases with the baryon density and it is found to be softer than that of NL3 but stiffer than that of IOPB-1, FSUGarnet, and Big Apple models.

B. Neutron star properties

In Fig. 6 we display the variation of pressure with the energy density for the nucleonic matter in β equilibrium for the DBHP parametrization. The results are also compared

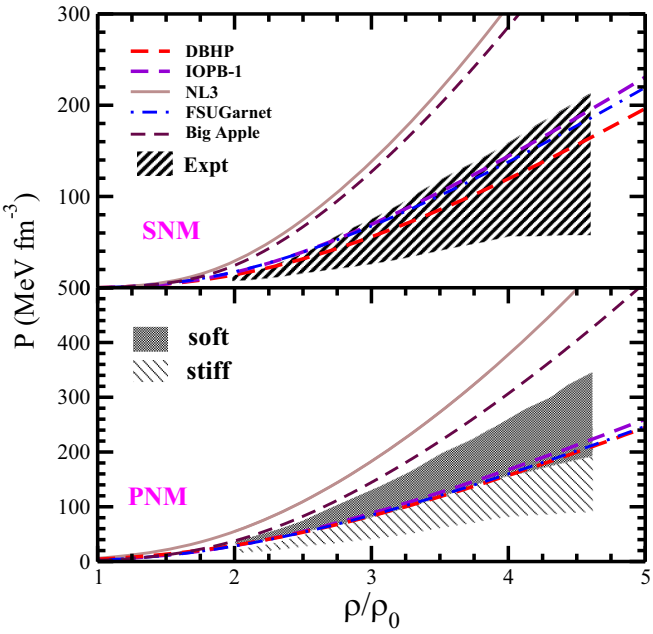

FIG. 4. Variation of pressure as a function of baryon density for SNM (upper panel) and PNM (lower panel) computed with DBHP parametrization along with NL3, IOPB-1, FSUGarnet, and Big Apple models. The shaded region represents the experimental data taken from Ref. [27].

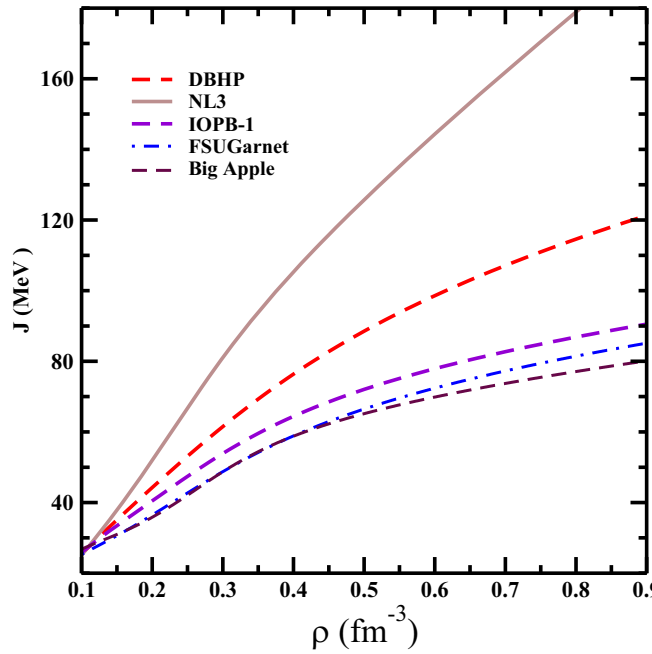

FIG. 5. The density-dependent symmetry energy plotted as a function of baryon density for the DBHP model. The results are also displayed for NL3, IOPB-1, FSUGarnet, and Big Apple parameter sets.

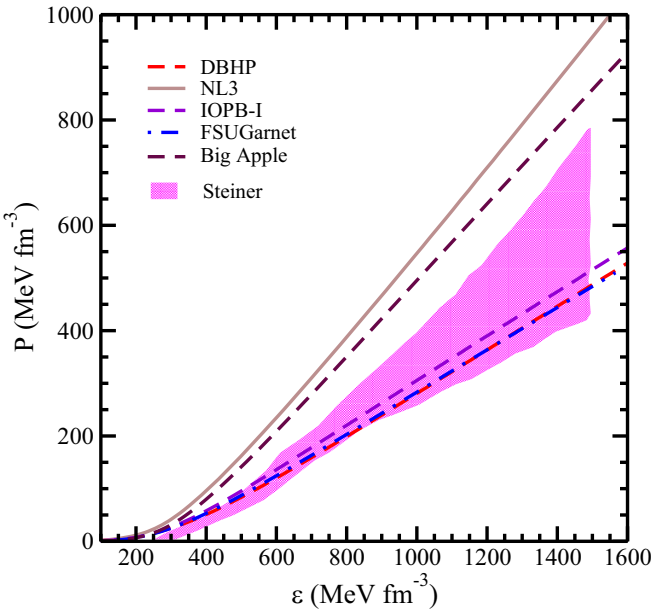

FIG. 6. Variation of pressure as a function of energy density for the DBHP parameter set. EOSs computed with NL3, IOPB-1, FSUGarnet, and Big Apple models are also shown for comparison. The shaded region represents the observational constraints taken from Ref. [56].

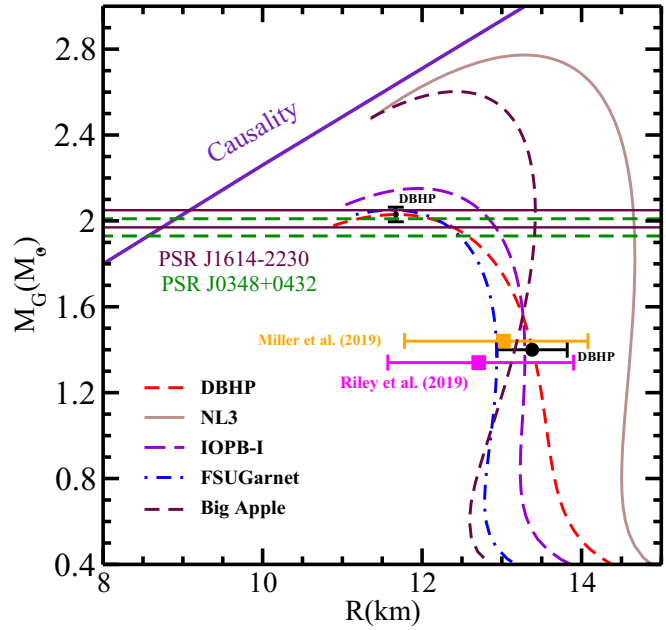

FIG. 7. Relationship between neutron star mass and its radius for DBHP parametrization. The results are compared with NL3, IOPB-1, FSUGarnet, and Big Apple parameters.

with those obtained for parameter sets. The shaded region represents the observational constraints at $r_{\rm ph} = R$ with the 2σ uncertainty [56]. Here $r_{\rm ph}$ and R are the photospheric and neutron star radius, respectively. It is clear that the EOSs computed with our DBHP parameter set are consistent with the EOSs obtained by Steiner *et al.* [56].

The EOSs obtained by the DBHP and IOPB-1 parametrizations are softer and lie in the allowed shaded region that represents the observational constraints taken from Ref. [56]. The EOS obtained with the NL3 parameter set is much stiffer than those obtained with the DBHP and IOPB-1 parameter sets and ruled out by the observational constraints [56]. The stiffness of the EOS for NL3 may be attributed to its very high value of compressibility (K), its symmetry energy coefficient (J), and its slope of symmetry energy (L) as shown in Table III. The mass and radius of a neutron star are obtained by solving the Tolman-Oppenheimer-Volkoff (TOV) equations [59,60] given as

$$\frac{dP(r)}{dr} = -\frac{\{\epsilon(r) + P(r)\}\{4\pi r^3 P(r) + m(r)\}}{r^2(1 - 2m(r)/r)}, \tag{16}$$

$$\frac{dm}{dr} = 4\pi r^2 \epsilon(r), \tag{17}$$

$$m(r) = 4\pi \int_0^r dr r^2 \epsilon(r) \tag{18}$$

where $P(r)$ is the pressure at radial distance r and $m(r)$ is the mass of neutron stars enclosed in the sphere of radius r. The EOS for the crust region is taken from Ref. [61]. In Fig. 7 we present our results for the gravitational mass of a static neutron star and its radius for DBHP and other parametrizations.

It is observed that the maximum gravitational mass of the static neutron star for the DBHP parameter set is 2.03 $M_\odot$, which is in good agreement with the mass constraints from the GW170817 event and pulsars PSRJ1614-2230, $PSRJ0348 + 0432$, and $PSRJ0740 + 6620$ [16,41,57,58,62]. The radius ($R_{1.4}$) of the canonical mass is 13.39 km for the DBHP parametrization, which satisfies the radius constraints from NICER [57,58,63]. The value of $R_{1.4}$ for the NL3 parametrization is 14.61 km which seems to rule out the constraints for $R_{1.4}$ extracted from Ref. [63].

The tidal deformability Λ rendered by the companion stars on each other in a binary system can provide remarkable pieces of information on the EOS of neutron stars [64,65]. The tidal influences of its companion in the BNS system will deform neutron stars in the binary system, and the resulting change in the gravitational potential modifies the BNS orbital motion and its corresponding gravitational wave (GW) signal. This effect on GW phasing can be parametrized by the dimensionless tidal deformability parameter $\Lambda_i = \lambda_i/M_i^5$, $i = 1$ and 2. For each neutron star, its quadrupole moment $\mathcal{Q}_{j,k}$ must be related to the tidal field $\mathcal{E}_{j,k}$ caused by its companion as $\mathcal{Q}_{j,k} = -\lambda \mathcal{E}_{j,k}$, where j and k are spatial tensor indices. The dimensionless tidal deformability parameter Λ of a static, spherically symmetric compact star depends on the neutron star compactness parameter C and a dimensionless quadrupole Love number k_2 as, $\Lambda = \frac{2}{3} k_2 C^{-5}$. The Λ critically parametrizes the deformation of neutron stars under the given tidal field; therefore, it should depend on the EOS of nuclear dense matter. To measure the Love number k_2 along with the evaluation of the TOV equations we have to compute $y_2 = y(R)$ with the initial boundary condition $y(0) = 2$ from

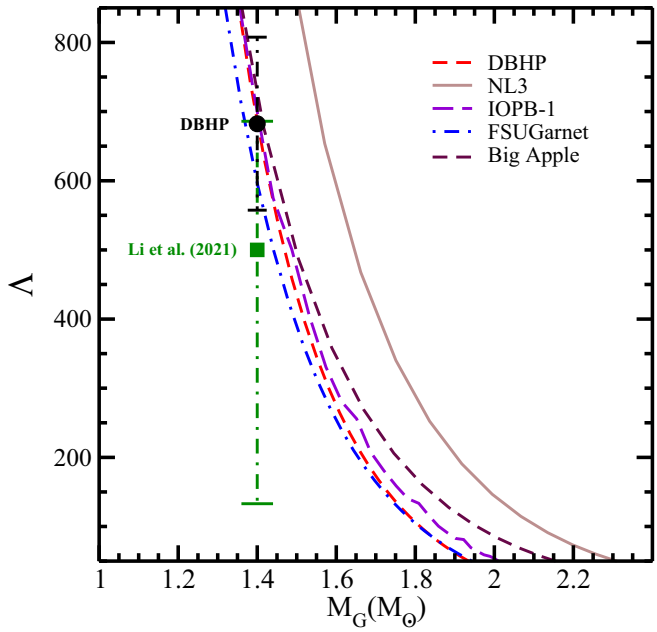

FIG. 8. Variation of dimensionless tidal deformability (Λ) with respect to gravitational mass for DBHP parametrization. The results for NL3, IOPB-1, FSUGarnet, and Big Apple parameters are also shown.

the first-order differential equation [64–67] simultaneously:

$$y' = \frac{1}{r}\{-r^2 Q - ye^{\lambda}[1 + 4\pi G r^2(P - \mathcal{E})] - y^2\}, \tag{19}$$

$$Q \equiv 4\pi G e^{\lambda}\left(5\mathcal{E} + 9P + \frac{\mathcal{E}+P}{c_s^2}\right) - 6\frac{e^{\lambda}}{r^2} - \nu'^2, \tag{20}$$

$$e^{\lambda} \equiv \left(1 - \frac{2Gm}{r}\right)^{-1}, \tag{21}$$

$$\nu' \equiv 2Ge^{\lambda}\left(\frac{m + 4\pi P r^3}{r^2}\right). \tag{22}$$

First, we get the solutions of Eq. (19) with the boundary condition $y_2 = y(R)$, and then the electric tidal Love number k_2 is calculated from the expression as

$$k_2 = \frac{8}{5}C^5(1-2C)^2[2C(y_2-1) - y_2 + 2] \times \Big\{2C[4(y_2+1)C^4 + (6y_2-4)C^3 + (26-22y_2)C^2 + 3(5y_2-8)C - 3y_2 + 6] - 3(1-2C)^2 \times [2C(y_2-1) - y_2 + 2]\log\left(\frac{1}{1-2C}\right)\Big\}^{-1}. \tag{23}$$

Figure 8 shows the results of the dimensionless tidal deformability Λ as a function of gravitational mass for neutron stars for DBHP and other parametrizations. The value of Λ decreases with an increase in the gravitational mass of the neutron star and reduces to a very small value at the maximum mass. The value of $\Lambda_{1.4}$ obtained for the canonical mass with DBHP parameters is 682 ± 125, which satisfies the finding from the GW170817 event [3,68,69] for the EOS of dense nuclear matter.

It is noteworthy that our analysis of tidal deformability ($\Lambda_{1.4}$) lies within the constraint ($\Lambda_{1.4} \leqslant 800$) for the GW170817 event [68], but the value of $\Lambda_{1.4}$ obtained for the DBHP model (682) has marginal overlap with the revised limit $\Lambda_{1.4} \leqslant 580$ within 1σ uncertainty [18]. This is attributed to the impact of the inclusion of PREX-II data in our fit, which produces stiff symmetry energy with the density slope $L = 83.9$ MeV. We are looking forward to the possibility that new terrestrial experiments and astrophysical observations may impose tighter bounds.

In Table IV, we present the results for the various properties of static stars with DBHP parametrization. The theoretical uncertainties calculated for the properties using Eqs. (13) and (14) are also listed. Results obtained with other parameter sets are also shown for comparison. We obtain very small theoretical uncertainties for the maximum mass $M_{\max}$ (1.9%), the maximum mass radius $R_{\max}$ (2.5%), and the radius $R_{1.4}$ (3%) of a neutron star. The small uncertainties might be attributed to the fact that the inclusion of $M_{\max}$ in the fit data constrain the high-density regime of the EOS. A relatively large uncertainty ($\approx$18%) is obtained for $\Lambda_{1.4}$. This is due to the fact that $\Lambda \propto R^5$, which indicates that precise measurement of tidal

TABLE IV. The properties of nonrotating neutron stars along with theoretical uncertainties obtained for the DBHP parameter set. Results are also compared with the other parameter sets. $M_{\max}$ and $R_{\max}$ denote the maximum gravitational mass and corresponding radius, respectively. The values for $R_{1.4}$ and $\Lambda_{1.4}$ denote the radius and the dimensionless tidal deformability at 1.4 $M_{\odot}$

EOS	$M_{\max}$ ($M_{\odot}$)	$R_{\max}$ (km)	$R_{1.4}$ (km)	$\Lambda_{1.4}$
DBHP	2.03 ± 0.04	11.68 ± 0.29	13.39 ± 0.41	682 ± 125
NL3	2.77	13.27	14.61	1254
IOPB-I	2.15	11.95	13.28	694
FSUGarnet	2.06	11.70	12.86	624
Big Apple	2.6	12.41	12.96	717

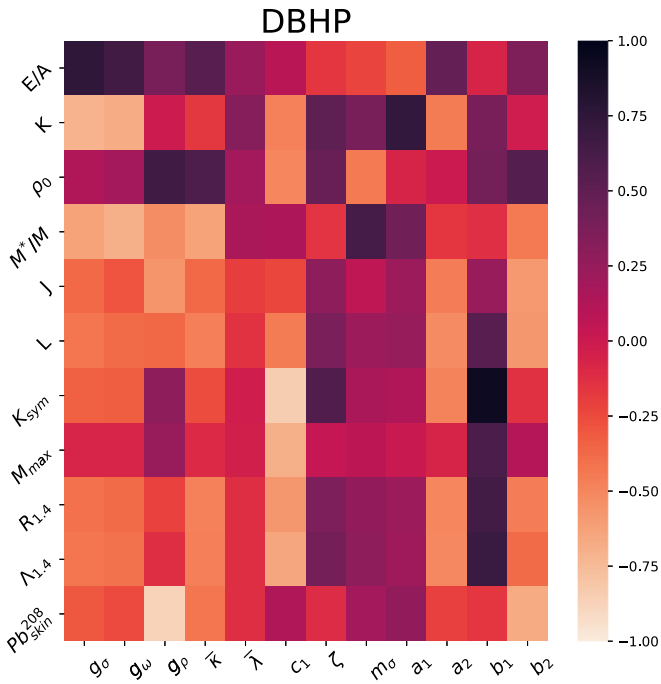

FIG. 9. Correlation coefficients between the model parameters and a set of neutron star observables as well as the bulk properties of nuclear matter at the saturation density for DBHP parametrization (see text for details).

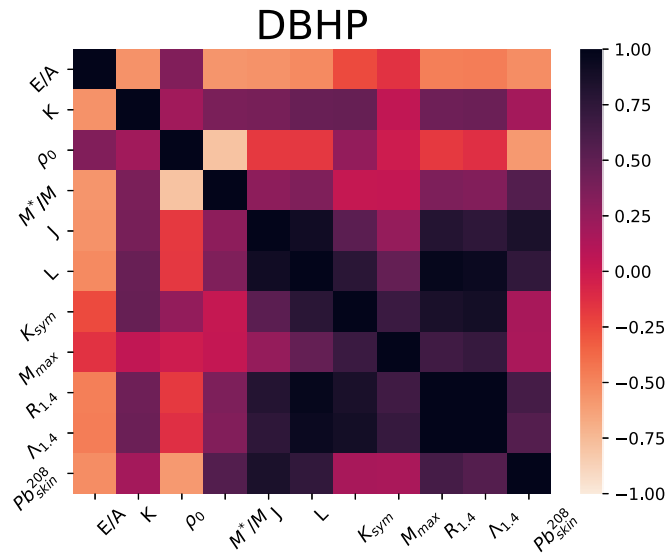

FIG. 10. Correlation coefficients for bulk nuclear matter and neutron star properties and neutron skin of ^{208}Pb for DBHP parametrization.

deformability can constrain the NS radius in narrow bounds. Indeed it is believed that no terrestrial experiment can reliably constrain the EOS of a neutron star [3].

C. Correlations of nuclear matter, neutron star properties, and model parameters

We now discuss the correlation coefficients, shown in Fig. 9, between the model parameters and the nuclear matter properties, the neutron skin thickness of the ^{208}Pb nucleus, and the NS observables. The isoscalar nuclear matter properties like E/A, K, and $M*/M$ show strong correlations with isoscalar parameters g_σ, g_ω, and $\overline{\kappa}$. It can also be observed from Fig. 9 that the symmetry energy slope parameter (L) can be constrained by the coupling parameter a_2, b_1, and b_2 along with the coupling parameter g_ρ as suggested by their correlations. The value of $\Delta r_{\rm np}$ is found to be well constrained by the parameters g_ρ and b_2 because they have strong correlations. This study is quite consistent with results reported in Refs. [33,35]. Finally, we discuss the correlations between neutron star observables and Lagrangian model parameters as shown in Fig. 9. A strong correlation between the maximum neutron star mass and the ω-meson self-coupling parameter ζ is missing in the case of the DBHP model parametrization. The $M_{\rm max}$ values display moderate correlations with the isovector coupling parameters c_1 and b_1. A large maximum mass may be generated either by having a stiff EOS for SNM or a stiff symmetry energy. If the symmetry energy is soft, then one must stiffen the EOS of SNM, which can be done by tuning the parameter ζ. However, the symmetry energy of the DBHP model is stiff as shown by Fig. 5. The symmetry energy slope parameter at saturation density is found to be 83.9 MeV. The stiff symmetry energy thereby weakens the correlation between ζ and $M_{\rm max}$. This suggests that the maximum mass results from a competition between ζ and L. This further implies that the parameter ζ should be well correlated to c_1 and b_1, and this is what is exactly reflected from the correlations shown in Fig. 1. The values of L and $K_{\rm sym}$ are found to be constrained by the parameters c_1 and b_1.

Finally, in Fig. 10 we display the correlation coefficients between the properties of nuclear matter, neutron star, and neutron skin thickness of ^{208}Pb. A strong correlation of the neutron skin thickness of the ^{208}Pb nucleus with J, L, $R_{1.4}$, and $\Lambda_{1.4}$ is observed. As per the expectation, the radius $R_{1.4}$ is found to have a strong correlation with J and L. These findings are quite in harmony with the results reported in Refs. [33,35]. The curvature of the symmetry energy ($K_{\rm sym}$) is also found to have a strong correlation with $R_{1.4}$ and $\Lambda_{1.4}$.

V. SUMMARY

The newly generated interaction DBHP for the relativistic mean field model has been generated by keeping in view the PREX-II data for neutron skin in the ^{208}Pb nucleus, astrophysical constraints in addition to those usually employed, like binding energy and charge radii for finite nuclei, and empirical data on nuclear matter at the saturation density. We have included all possible self and mixed interactions between σ, ω, and ρ mesons up to the quartic order so that the coupling parameters obey the naturalness behavior as imposed by the effective field theory [28]. The covariance analysis enabled us to assess the statistical uncertainties in the estimation of the model parameters and observables of interest as well as the correlations among them. The DBHP parameter set is obtained such that it reproduces the ground-state properties of the finite nuclei and the bulk nuclear matter properties and also satisfies the constraints

of mass and radius of the neutron star and its dimensionless deformability Λ from recent astrophysical observations [18,19,56,63]. The rms errors in the total binding energies and charge rms radii for finite nuclei included in our fit for the DBHP parametrization are 2.1 MeV and 0.02 fm, respectively. The bulk nuclear matter properties obtained are well consistent with the current empirical data [3,55]. The maximum gravitational mass and radius ($R_{1.4}$) of the neutron star come out to be 2.03 ± 0.04 M$\odot$ and 13.39 ± 0.41 km respectively. The value of $\Lambda_{1.4}$ that is equal to 682 ± 125 for the DBHP parametrization also satisfies the constraints for the GW170817 event [68] and those reported in Refs. [3,69]. The parametrization generated in consideration of the PREX-II data produces a stiff symmetry energy coefficient and its density dependence leads to $\Lambda_{1.4} = 682 \pm 125$, which has marginal overlap with the revised constraint [18]. We are looking forward to the possibility that new terrestrial experiments and astrophysical observations may put more stringent constraints on the density dependence of the symmetry energy.

ACKNOWLEDGMENTS

V.T. is thankful to Himachal Pradesh University for providing the computational facility and the Department of Science & Technology (Government of India) for providing financial assistance (DST/INSPIRE Fellowship/2017/IF170302) under the Junior/Senior Research Fellowship scheme. C.M. acknowledges partial support from the IN2P3 Master Project "NewMAC".

[1] J. M. Lattimer and M. Prakash, Science **304**, 536 (2004).
[2] C. J. Horowitz and J. Piekarewicz, Neutron Star Structure and the Neutron Radius of ^{208}Pb, Phys. Rev. Lett. **86**, 5647 (2001).
[3] B. T. Reed, F. J. Fattoyev, C. J. Horowitz, and J. Piekarewicz, Implications of PREX-2 on the Equation of State of Neutron-Rich Matter, Phys. Rev. Lett. **126**, 172503 (2021).
[4] F. J. Fattoyev, J. Piekarewicz, and C. J. Horowitz, Neutron Skins and Neutron Stars in the Multimessenger Era, Phys. Rev. Lett. **120**, 172702 (2018).
[5] S. K. Dhiman, R. Kumar, and B. K. Agrawal, Nonrotating and rotating neutron stars in the extended field theoretical model, Phys. Rev. C **76**, 045801 (2007).
[6] B. K. Pradhan, D. Chatterjee, R. Gandhi, and J. Schaffner-Bielich, Role of vector self-interaction in neutron star properties, Nucl. Phys. A **1030**, 122578 (2022).
[7] V. Thakur, R. Kumar, P. Kumar, V. Kumar, B. K. Agrawal, and S. K. Dhiman, Relativistic mean field model parametrizations in the light of GW170817, GW190814, and PSR J0740+ 6620, Phys. Rev. C **106**, 025803 (2022).
[8] V. Thakur, R. Kumar, P. Kumar, V. Kumar, M. Kumar, C. Mondal, B. K. Agrawal, and S. K. Dhiman, Effects of an isovector scalar meson on the equation of state of dense matter within a relativistic mean field model, Phys. Rev. C **106**, 045806 (2022).
[9] S. Thakur, V. Thakur, R. Kumar, and S. K. Dhiman, Structural properties of rotating hybrid compact stars with color-flavor-locked quark matter core and their tidal deformability, Eur. Phys. J. A **58**, 93 (2022).
[10] P. Haensel, A. Yu. Potekhin, and D. G. Yakovlev, *Neutron Stars 1: Equation of State and Structure*, Astrophysics and Space Science Library Vol. 326 (Springer Science & Business Media, New York, 2007).
[11] J. M. Lattimer, Neutron stars, Gen. Relativ. Gravitation **46**, 1713 (2014).
[12] G. Baym, T. Hatsuda, T. Kojo, P. D. Powell, Y. Song, and T. Takatsuka, From hadrons to quarks in neutron stars: a review, Rep. Prog. Phys. **81**, 056902 (2018).
[13] K. Hebeler, J. M. Lattimer, C. J. Pethick, and A. Schwenk, Constraints on Neutron Star Radii Based on Chiral Effective Field Theory Interactions, Phys. Rev. Lett. **105**, 161102 (2010).
[14] K. Hebeler, J. M. Lattimer, C. J. Pethick, and A. Schwenk, Equation of state and neutron star properties constrained by nuclear physics and observation, Astrophys. J. **773**, 11 (2013).
[15] J. M. Lattimer, The nuclear equation of state and neutron star masses, Annu. Rev. Nucl. Part. Sci. **62**, 485 (2012).
[16] P. B. Demorest, T. Pennucci, S. M. Ransom, M. S. E. Roberts, and J. W. T. Hessels, A two-solar-mass neutron star measured using Shapiro delay, Nature (London) **467**, 1081 (2010).
[17] J. Antoniadis, P. C. C. Freire, N. Wex, T. M. Tauris, R. S. Lynch, M. H. van Kerkwijk, M. Kramer, C. Bassa, V. S. Dhillon, T. Driebe *et al.*, A massive pulsar in a compact relativistic binary, Science **340**, 1233232 (2013).
[18] B. P. Abbott, R. Abbott, T. D. Abbott, F. Acernese, K. Ackley, C. Adams, T. Adams, P. Addesso, R. X. Adhikari, V. B. Adya *et al.*, GW170817: Measurements of Neutron Star Radii and Equation of State, Phys. Rev. Lett. **121**, 161101 (2018).
[19] B. P. Abbott, R. Abbott, T. D. Abbott, F. Acernese, K. Ackley, C. Adams, T. Adams, P. Addesso, R. X. Adhikari, V. B. Adya *et al.*, Properties of the Binary Neutron Star Merger GW170817, Phys. Rev. X **9**, 011001 (2019).
[20] Z. Arzoumanian, A. Brazier, S. Burke-Spolaor, S. Chamberlin, S. Chatterjee, B. Christy, J. M. Cordes, N. J. Cornish, F. Crawford, H. T. Cromartie *et al.*, The NANOGrav 11-year data set: High-precision timing of 45 millisecond pulsars, Astrophys. J., Suppl. Ser. **235**, 37 (2018).
[21] M. C. Miller, F. K. Lamb, A. J. Dittmann, S. Bogdanov, Z. Arzoumanian, K. C. Gendreau, S. Guillot, A. K. Harding, W. C. G. Ho, J. M. Lattimer, R. M. Ludlam, S. Mahmoodifar, S. M. Morsink, P. S. Ray, T. E. Strohmayer, K. S. Wood, T. Enoto, R. Foster, T. Okajima, G. Prigozhin *et al.*, PSR $J0030+0451$ mass and radius from *NICER* data and implications for the properties of neutron star matter, Astrophys. J. **887**, L24 (2019).
[22] T. E. Riley, A. L. Watts, S. Bogdanov, P. S. Ray, R. M. Ludlam, S. Guillot, Z. Arzoumanian, C. L. Baker, A. V. Bilous, D. Chakrabarty, K. C. Gendreau, A. K. Harding, W. C. G. Ho, J. M. Lattimer, S. M. Morsink, and T. E. Strohmayer, A *NICER* view of PSR $J0030+0451$: Millisecond pulsar parameter estimation, Astrophys. J. Lett. **887**, L21 (2019).
[23] G. Raaijmakers, T. E. Riley, A. L. Watts, S. K. Greif, S. M. Morsink, K. Hebeler, A. Schwenk, T. Hinderer, S. Nissanke, S. Guillot, Z. Arzoumanian, S. Bogdanov, D. Chakrabarty, K. C.

Gendreau, W. C. G. Ho, J. M. Lattimer, R. M. Ludlam, and M. T. Wolff, A *NICER* view of PSR $J0030 + 0451$: Implications for the dense matter equation of state, Astrophys. J. **887**, L22 (2019).

[24] D. Adhikari, H. Albataineh, D. Androic, K. Aniol, D. S. Armstrong, T. Averett, C. A. Gayoso, S. Barcus, V. Bellini, R. S. Beminiwattha *et al.*, Accurate Determination of the Neutron Skin Thickness of ^{208}Pb through Parity-Violation in Electron Scattering, Phys. Rev. Lett. **126**, 172502 (2021).

[25] J. M. Lattimer and M. Prakash, Neutron star structure and the equation of state, Astrophys. J. **550**, 426 (2001).

[26] R. W. Romani, D. Kandel, A. V. Filippenko, T. G. Brink, and W. Zheng, PSR J0952-0607: The fastest and heaviest known galactic neutron star, Astrophys. J. Lett. **934**, L17 (2022).

[27] P. Danielewicz, Science **298**, 1592 (2002).

[28] R. J. Furnstahl, B. D. Serot, and H.-B. Tang, A chiral effective Lagrangian for nuclei, Nucl. Phys. A **615**, 441 (1997).

[29] R. Kumar, B. K. Agrawal, and S. K. Dhiman, Effects of ω meson self-coupling on the properties of finite nuclei and neutron stars, Phys. Rev. C **74**, 034323 (2006).

[30] T. J. Bürvenich, D. G. Madland, and P.-G. Reinhard, Adjustment studies in self-consistent relativistic mean-field models, Nucl. Phys. A **744**, 92 (2004).

[31] S. Kirkpatrick, Optimization by simulated annealing: Quantitative studies, J. Stat. Phys. **34**, 975 (1984).

[32] J. Dobaczewski, W. Nazarewicz, and P. G. Reinhard, Error estimates of theoretical models: a guide, J. Phys. G: Nucl. Part. Phys. **41**, 074001 (2014).

[33] W.-C. Chen and J. Piekarewicz, Searching for isovector signatures in the neutron-rich oxygen and calcium isotopes, Phys. Lett. B **748**, 284 (2015).

[34] C. Mondal, B. K. Agrawal, and J. N. De, Constraining the symmetry energy content of nuclear matter from nuclear masses: A covariance analysis, Phys. Rev. C **92**, 024302 (2015).

[35] F. J. Fattoyev, C. J. Horowitz, J. Piekarewicz, and B. Reed, GW190814: Impact of a 2.6 solar mass neutron star on the nucleonic equations of state, Phys. Rev. C **102**, 065805 (2020).

[36] S. Brandt, *Statistical and Computational Methods in Data Analysis* (Springer, Berlin, 1997).

[37] P.-G. Reinhard and W. Nazarewicz, Information content of a new observable: The case of the nuclear neutron skin, Phys. Rev. C **81**, 051303(R) (2010).

[38] M. Wang, G. Audi, F. G. Kondev, W. J. Huang, S. Naimi, and X. Xu, The AME2016 atomic mass evaluation (II). Tables, graphs and references, Chin. Phys. C **41**, 030003 (2017).

[39] E. W. Otten, *Treatise on Heavy-Ion Science*, edited by D. A. Bromley (Springer, Berlin, 1989), Vol. 8, p. 517.

[40] H. Vries, C. W. Jager, and C. Vries, Nuclear-charge-density distribution parameters from elastic electron scattering, At. Data Nucl. Data Tables **36**, 495 (1987).

[41] L. Rezzolla, E. R. Most, and L. R. Weih, Using gravitational-wave observations and quasi-universal relations to constrain the maximum mass of neutron stars, Astrophys. J. Lett. **852**, L25 (2018).

[42] P. Ring and P. Schuck, *The Nuclear Many-Body Problem* (Springer Science & Business Media, New York, 1980).

[43] S. Karatzikos, A. V. Afanasjev, G. A. Lalazissis, and P. Ring, The fission barriers in actinides and superheavy nuclei in covariant density functional theory, Phys. Lett. B **689**, 72 (2010).

[44] M. Wang, W. J. Huang, F. G. Kondev, G. Audi, and S. Naimi, The AME 2020 atomic mass evaluation (II). Tables, Graphs and References, Chin. Phys. C **45**, 030003 (2021).

[45] G. A. Lalazissis, J. König, and P. Ring, New parametrization for the Lagrangian density of relativistic mean field theory, Phys. Rev. C **55**, 540 (1997).

[46] B. Kumar, S. K. Patra, and B. K. Agrawal, New relativistic effective interaction for finite nuclei, infinite nuclear matter, and neutron stars, Phys. Rev. C **97**, 045806 (2018).

[47] W. G. Newton and G. Crocombe, Nuclear symmetry energy from neutron skins and pure neutron matter in a Bayesian framework, Phys. Rev. C **103**, 064323 (2021).

[48] J. Xu and P. Papakonstantinou, Bayesian inference of finite-nuclei observables based on the kids model, Phys. Rev. C **105**, 044305 (2022).

[49] H. Gil, P. Papakonstantinou, and C. H. Hyun, Constraints on the curvature of nuclear symmetry energy from recent astronomical data within the kids framework, Int. J. Mod. Phys. E **31**, 2250013 (2022).

[50] D. Adhikari *et al.*, Phys. Rev. Lett. **129**, 042501 (2022).

[51] E. Yuksel and N. Paar, Implications of parity-violating electron scattering experiments on ^{48}Ca (crex) and ^{208}Pb (PREX-II) for nuclear energy density functionals, Phys. Lett. B **836**, 137622 (2023).

[52] P.-G. Reinhard, X. Roca-Maza, and W. Nazarewicz, Combined Theoretical Analysis of the Parity-Violating Asymmetry for ^{48}Ca and ^{208}Pb, Phys. Rev. Lett. **129**, 232501 (2022).

[53] J. Piekarewicz, The nuclear physics of neutron stars, arXiv2209.14877v2 (2022).

[54] G. Colo, U. Garg, and H. Sagawa, Symmetry energy from the nuclear collective motion: constraints from dipole, quadrupole, monopole and spin-dipole resonances, Eur. Phys. J. A **50**, 26 (2014).

[55] J. Piekarewicz, Symmetry energy constraints from giant resonances: A relativistic mean-field theory overview, Eur. Phys. J. A **50**, 25 (2014).

[56] A. W. Steiner, J. M. Lattimer, and E. F. Brown, The equation of state from observed masses and radii of neutron stars astrophys, Astrophys. J. **722**, 33 (2010).

[57] T. E. Riley, A. L. Watts, P. S. Ray, S. Bogdanov, S. Guillot, S. M. Morsink, A. V. Bilous, Z. Arzoumanian, D. Choudhury, J. S. Deneva *et al.*, A nicer view of the massive pulsar PSR J0740+6620 informed by radio timing and XMM-Newton spectroscopy, Astrophys. J. Lett. **918**, L27 (2021).

[58] M. C. Miller, F. K. Lamb, A. J. Dittmann, S. Bogdanov, Z. Arzoumanian, K. C. Gendreau, S. Guillot, W. C. G. Ho, J. M. Lattimer, M. Loewenstein *et al.*, The radius of PSR J0740+6620 from NICER and XMM-Newton data, Astrophys. J. Lett. **918**, L28 (2021).

[59] J. R. Oppenheimer and G. M. Volkoff, On massive neutron cores, Phys. Rev. **55**, 374 (1939).

[60] R. C. Tolman, Static solutions of einstein's field equations for spheres of fluid, Phys. Rev. **55**, 364 (1939).

[61] Y. Sugahara and H. Toki, Relativistic mean-field theory for unstable nuclei with non-linear σ and ω terms, Nucl. Phys. A **579**, 557 (1994).

[62] E. Fonseca, T. T. Pennucci, J. A. Ellis, I. H. Stairs, D. J. Nice, S. M. Ransom, P. B. Demorest, Z. Arzoumanian, K. Crowter, T. Dolch *et al.*, The nanograv nine-year data set: Mass and geometric measurements of binary millisecond pulsars, Astrophys. J. **832**, 167 (2016).

[63] E. Annala, T. Gorda, A. Kurkela, and A. Vuorinen, Gravitational-Wave Constraints on the Neutron-Star-Matter Equation of State, Phys. Rev. Lett. **120**, 172703 (2018).

[64] T. Hinderer, Tidal love numbers of neutron stars, Astrophys. J. **677**, 1216 (2008).

[65] T. Hinderer, B. D. Lackey, R. N. Lang, and J. S. Read, Tidal deformability of neutron stars with realistic equations of state and their gravitational wave signatures in binary inspiral, Phys. Rev. D **81**, 123016 (2010).

[66] T. Hinderer, Erratum: "Tidal love numbers of neutron stars" (2008, ApJ, 677, 1216), Astrophys. J. **697**, 964 (2009).

[67] T. Damour and A. Nagar, Effective one body description of tidal effects in inspiralling compact binaries, Phys. Rev. D **81**, 084016 (2010).

[68] B. P. Abbott, R. Abbott, T. D. Abbott, F. Acernese, K. Ackley, C. Adams, T. Adams, P. Addesso, R. X. Adhikari, V. B. Adya *et al.*, GW170817: Observation of Gravitational Waves from a Binary Neutron Star Inspiral, Phys. Rev. Lett. **119**, 161101 (2017).

[69] Y. Li, H. Chen, D. Wen, and J. Zhang, Constraining the nuclear symmetry energy and properties of the neutron star from GW170817 by Bayesian analysis, Eur. Phys. J. A **57**, 1 (2021).